PAPER

Check for updates

An efficient screening strategy towards multifunctional catalysts for the simultaneous electroreduction of NO_3^-, NO_2^- and NO to NH_3†

Peng Lv,[ae] Donghai Wu,[a] Bingling He,[a] Xue Li,[a] Rui Zhu,[a] Gang Tang, [b] Zhansheng Lu, [c] Dongwei Ma [*ae] and Yu Jia [*ade]

Multifunctional electrocatalysts that simultaneously reduce all NO_x species (NO_3^-, NO_2^- and NO) to NH_3 can deliver superior efficiency compared with that for individual species. Herein, by using the first-principles method, an efficient strategy was proposed to screen NO_xRR multifunctional electrocatalysts, which focuses on the key protonation process of the essential NORR for the NO_xRR. Taking double-atom catalysts (DACs) with transition-metal dimer (M1/M2 = V, Cr, Mn, Fe, Co, Ni, and Cu) embedded N-doped graphene as examples, we showed that the proposed strategy was effective for electrocatalyst screening, and we identified Cu_2@NG as the best one, with rather low limiting potentials of −0.36, −0.32, and −0.30 V for the NO_3RR, NO_2RR, and NORR, respectively. Furthermore, a simple descriptor for evaluating electrocatalytic activity was established. And the physical mechanism in terms of the electronic structures was analyzed for the Cu_2 DAC case in view of NO activation. Finally, from the screening test in some 4d and 5d late transition-metal based DACs, the proposed strategy was confirmed to be feasible to find another NO_xRR multifunctional electrocatalyst. Our work provides a procedure for efficiently screening multifunctional electrocatalysts to simultaneously reduce all NO_x species to synthesize NH_3 and sheds light on the atomic mechanisms for NO_x electroreduction as well.

1. Introduction

For a long time, the production of valuable ammonia (NH_3) mainly has depended on the traditional Haber–Bosch process that occurs at high temperature and pressure and is extremely economically and environmentally unfriendly. Yet, researchers turned to the electrochemical N_2 reduction reaction (NRR) mimicking biological nitrogen fixation towards NH_3.[1–6] Due to the poor NRR performance resulting from the extremely inert N≡N bond, alternatively the electrochemical conversion of other important nitrogenous species, NO_x (NO_3^-, NO_2^- and NO), came into focus very recently. It turns out that this not only produces NH_3 beyond NRR under ambient conditions, but also removes the waste NO_x species.[7,8] In contrast, this denitrification process in nature reduces the NO_x species to N_2O by fungi and N_2 by bacteria.[9]

It should be noted that nitrate and nitrite ions usually coexist in waste water, such as contaminated groundwater, lakes, and coastal water, which also includes NO from biological denitrification.[9] In addition, the NO_x species can be easily obtained by the plasma activation of air.[10,11] To this end, developing multifunctional electrocatalysts that simultaneously reduce all the NO_x species promises higher conversion efficiency for NH_3 synthesis compared with monofunctional ones.[10,12,13] Up to now, existing research has mainly focused on monofunctional systems for individual species, while the design strategy of multifunctional catalysts for the NO_xRR has been lacking. As we all know, the NORR is an essential reaction for determining the performance of electrocatalysts for the electroreduction of NO_3^- and NO_2^- to NH_3.[14,15] Therefore, for the NO_xRR towards NH_3 instead of other by-products (H_2, N_2, and N_2O), the premise is to design an efficient NORR electrocatalyst with high activity and NH_3 selectivity.

Since the proposal of single-atom catalysts (SACs) by Zhang *et al.* in 2011,[16] they have also been confirmed to show high activity for NH_3 synthesis from the NORR, NO_2RR or NO_3RR (*i.e.*, Mg/Al/Ga/Co@NG,[17–19] Zr–C_2N,[20] Ru@C_3N_4,[21] and Ti/Zr@CN[22]). Unfortunately, the individual active site gives rise to their deficiency in multifunctional electrocatalytic ability to reduce all the NO_x species, which motivates us to design

[a]Key Laboratory for Special Functional Materials of Ministry of Education, School of Materials Science and Engineering, Henan University, Kaifeng 475004, China. E-mail: madw@henu.edu.cn; jiayu@henu.edu.cn

[b]Advanced Research Institute of Multidisciplinary Science, Beijing Institute of Technology, Beijing 100081, China

[c]School of Physics, Henan Normal University, Xinxiang 453007, China

[d]International Laboratory for Quantum Functional Materials of Henan, School of Physics, Zhengzhou University, Zhengzhou 450001, China

[e]Joint Center for Theoretical Physics, Center for Topological Functional Materials, Henan University, Kaifeng 475004, China

† Electronic supplementary information (ESI) available. See DOI: 10.1039/d2ta00192f

This journal is © The Royal Society of Chemistry 2022

J. Mater. Chem. A, 2022, **10**, 9707–9716 | 9707

multifunctional electrocatalysts. Given the flexibility of dual active sites in double-atom catalysts (DACs),[23–26] there are more possibilities to adjust their geometrical bridge configurations,[27] offering more opportunities to modulate the binding strength of reaction intermediates and then optimize the catalytic activity, selectivity and multifunctional ability.[28] For instance, compared with atomically dispersed single Fe and Ni catalysts, with the help of the synergetic effect of dual active sites, a bimetallic FeNi DAC exhibits outstanding multifunctional performance for the reversible oxygen evolution reaction and oxygen reduction reaction.[29] Furthermore, various DACs have been theoretically and experimentally confirmed to show high activity and selectivity for the NRR.[23,30–35] In view of these advantages, it is expected that DACs would be multifunctional electrocatalysts with the potential ability for reducing all NO_x species, which has not yet been reported.

Here, by using the first-principles method, we proposed an optimized strategy for screening multifunctional electrocatalysts to reduce all NO_x species. The screening strategy consists of the steps of "stability of catalyst", "NO adsorption", "NORR activity", and "NH_3 selectivity". We used the selection metric of "two steps of key hydrogenation process" to measure the "NORR activity", which is confirmed to be very effective. According to some late transition-metal based SACs with good electrocatalytic ability for the NO_2RR or NO_3RR in the experiment,[18,36–38] together with recently synthesized transition-metal dimer embedded N-doped graphene (M1M2@NG),[32,39–43] 28 DAC candidates were built (M1/M2 = V, Cr, Mn, Fe, Co, Ni, and Cu) for screening multifunctional electrocatalysts for the NO_xRR. Through firstly systematic screening for NORR electrocatalysts, the DAC of Cu_2@NG was identified as the best one due to its smallest limiting potential (U_L, −0.30 V) and high NH_3 selectivity. As expected, the catalytic merits of Cu_2@NG can be extended to the NO_2RR (U_L, −0.36 V) and NO_3RR (U_L, −0.32 V). Moreover, the electroreduction activity descriptor and physical mechanism in terms of electronic structures were analyzed. Our work provides an effective strategy to screen multifunctional electrocatalysts for the NO_xRR, by which a cost-efficient and stable candidate with desirable NH_3 activity and selectivity was identified.

2. Methods

All spin-polarized computations were carried out by the generalized gradient approximation (GGA) method with the Perdew–Burke–Ernzerhof (PBE) functional[44] based on density functional theory (DFT) implemented in the Vienna *ab initio* simulation package (VASP),[45,46] in which van der Waals (vdW) correction proposed by Grimme (DFT+D3) was chosen.[47] The plane-wave basis set with a cut-off energy of 450 eV was employed. The convergence thresholds of the total energy and the Hellmann–Feynman force are 10^{-5} eV and 0.02 eV Å^{-1}, respectively. A 7 × 7 supercell of graphene with a vacuum layer of ∼18 Å is used to avoid the interactions between periodic images for all calculations. Monkhorst–Pack meshes of 3 × 3 × 1 and 7 × 7 × 1 are adopted for structural optimization and calculation of densities of states (DOS), respectively.

The free energy change (ΔG) under the acidic medium (pH = 0) for each elementary reaction step was calculated based on the computational hydrogen electrode (CHE) model,[48–50] according to the following equation:

$$\Delta G = \Delta E + \Delta E_{ZPE} - T\Delta S$$

ΔE is the reaction energy from DFT calculations. ΔE_{ZPE} and $T\Delta S$ (T = 298.15 K) are the contributions of the zero-point energy and entropy to ΔG, respectively. E_{ZPE} and TS for the free molecules are taken from the NIST database,[51] and those of the adsorbed species were obtained based on the calculated vibrational frequencies and then with the VASPKIT code.[52] The limiting potential (U_L) is defined as $-\Delta G_{max}/e$, where ΔG_{max} is the free energy change of the potential-determining step (PDS). Due to the difference of formation energies from experimental and DFT results for HNO_3 and HNO_2, along with the energy difference of solvated NO_3^-/NO_2^- (aq) and HNO_3/HNO_2 (g), here ΔG ($*NO_3^-$) and ΔG ($*NO_2^-$) are correspondingly corrected based on their differences.

The hybrid model,[53,54] *i.e.*, the combination of explicit solvation model with two water molecules near the active site and continuum solvation model,[55] was used to investigate the solvation effect on the NO_xRR. The solvation effect doesn't change our conclusions about the screening of multifunctional electrocatalysts for the NO_xRR (for the details and results, see Note S1 in the ESI†). The pH effect was also considered from the viewpoints of thermodynamics and dynamics. The results show that Cu_2 and Ag_2 DACs are excellent acidic electrocatalysts to multifunctionally reduce all the NO_x species (for the details and results, see Note S2 in the ESI†). The thermal stability of Cu_2 and Ag_2 DACs was examined by *ab initio* molecular dynamics simulations[56] for 10 ps with the current 7 × 7 supercells of graphene (for the details and results, see Note S3 in the ESI†).

3. Results and discussion

For DACs, graphene containing nitrogen (NG) is an excellent substrate with anchoring sites for metal dimer deposition. Some DACs of Fe_2@NG,[39] FeCo@NG,[40,41] FeNi@NG,[24] and CoNi@NG[42] have been definitely determined experimentally and exhibit excellent catalytic performances for the O_2 reduction reaction (ORR). In addition, a few M1M2@NG DACs also possess a great N_2 reduction ability with NH_3 selectivity.[5,32,43] In this regard, M1M2@NG DACs may be promising electrocatalyst candidates for the NO_xRR including both the hydrogenation of N and O atoms in the NO_x species. Given that the NORR is the essential reaction of the NO_xRR, we will firstly consider the design of a NORR electrocatalyst from the M1M2@NG system. The atomic structure of M1M2@NG is presented in Fig. 1a, where each metal atom is tetra-coordinated with three N atoms and another metal atom. Both the homonuclear and heteronuclear cases were considered for 3d metals (M1/M2 = V, Cr, Mn, Fe, Co, Ni, and Cu), leading to 28 kinds of DAC candidates. The deposited metal dimers are well within the atomic plane of graphene, probably thanks to the large size of the pore decorated with the edge N atoms. Our recent studies[5,34] showed that
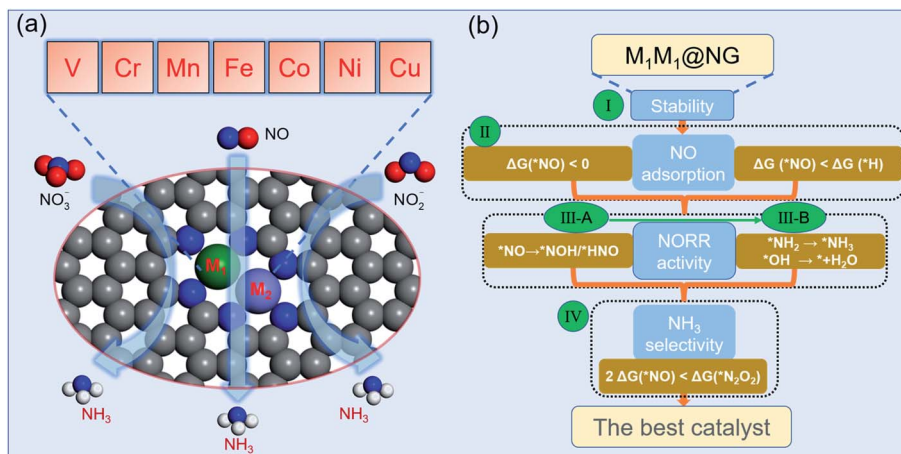
Fig. 1 (a) The atomic structure of M1M2@NG DACs (M1/M2 = V, Cr, Mn, Fe, Co, Ni, and Cu). (b) The optimized strategy for screening NORR electrocatalysts including four stepwise selection principles. The third criterion consists of ''two steps of key hydrogenation process''.

the metal dimer in DACs can provide a bridge active site for the adsorption of N_2 and relevant intermediates, which is beneficial for molecular activation and its further hydrogenation.

According to the NORR characteristics,[12,18,57–59] we comprehensively proposed four stepwise selection principles (Fig. 1b) for the best NORR electrocatalysts: (I) the thermodynamic stability of the catalyst for the feasibility of experimental realization, (II) stable adsorption of molecular NO for activation, and superiority to H, (III) high NORR activity to NH_3 with low ΔG_{max} (here the threshold value (G_T) was set as 0.4 eV, i.e., $U_L \geq 0.4$ V), and (IV) great NH_3 selectivity with inhibitive ability of other products (N_2 and N_2O).[14] Particularly, for the third criterion, we used the selection metric of "two steps of key hydrogenation process" to measure the catalytic activity for the NORR, rather than calculating the overall reaction pathway of numerous candidates.

We have investigated the feasibility of experimental realization of these 28 DACs based on the calculated formation energies and binding energies.[5] The results showed that their formation energies (about 2.8–4.3 eV) are lower than or comparable with those of several synthesized ones (i.e. FeNi@NG,[24] Fe_2@NG,[39] FeCo@NG,[40,41] and CoNi@NG[42]). And their more negative binding energies (about −9.5 to −13.5 eV) suggest that highly stable complexes can be formed by depositing metal atoms onto an N-doped porous graphene support. As the first step of the NORR, the adsorption and activation of NO on M1M2@NG DACs were investigated. Various kinds of NO adsorption configurations were initially studied to determine the favorable one. The most stable adsorption configurations are summarized in Fig. S1.† It was found that most stable species over M1M2@NG prefer to stay over the metal atoms with three representative configurations (Fig. 2a): (1) the side-on pattern with the N atom binding with both metal atoms and the O atom with one metal atom (NO^{α}), and (2) the end-on pattern with the N atom binding with both metal atoms (NO^{β}_{M1M2}) or one metal atom (NO^{β}_{M1}).

Interestingly, most DACs adopt an end-on configuration for *NO (NO^{β}_{M1} mainly for Ni and Cu-alloy DACs), while only V_2,

VCr, and VMn@NG DACs prefer to adopt the side-on NO^{α} configuration (Fig. S1†), which may result from the fact that V_2, VCr, and VMn dimers have fewer d-orbital electrons. From the relationship between the charge transfer (Q, e) and N–O bond length in Fig. 2b, the side-on NO^{α} configurations transfer more electrons (1.00–1.04 e) from the DAC support to the *NO and make the length of the N–O bond longer (1.35–1.38 Å from 1.15 Å in the free NO molecule). For each NO^{β}_{M1} and NO^{β}_{M1M2} end-on configuration, there is a nearly linear correlation between the electron transfer and the length of the N–O bond. Correspondingly, the NO^{β}_{M1} configurations have relatively less electron transfer between the *NO and DACs than NO^{β}_{M1M2} configurations, resulting in the difference of N–O bond lengths. From the free energy change for *NO (Fig. 2c), we can find that *NO over V_2, VCr, and VMn DACs with a side-on configuration has smaller ΔG values due to the higher activation of *NO with a large N–O bond length than that with an end-on configuration. Moreover, all the DACs have negative ΔG values for *NO with enlarging N–O bond, indicating the chemical adsorption and activation of *NO. The negative ΔG has a linear relationship with the total number of d-orbital valence electrons ($N_{d-orbital}$) of free metal-dimer atoms (Fig. S2†): more $N_{d-orbital}$ corresponds to less negative ΔG. Thus, the Cu_2 DAC has the least negative ΔG for the NO configuration among these DAC systems, while it still possesses the capture ability for NO molecules under ambient conditions.

Since H adsorption is generally strong on most bulk metal surfaces, the active site of metal surfaces can be easily blocked by the covered *H to inhibit electrocatalytic reduction, such as for the NRR.[60] Here also for the NORR, NO adsorption has to compete with the H adsorption over active sites. Based on this, we calculated the H adsorption on various DACs and the comparison results of ΔG (*H) and ΔG (*NO) are organized in Fig. 2d. We found that all the electrocatalysts have more negative ΔG values for *NO than that for *H over the corresponding DACs, indicating that they have a strong binding capability for NO to suppress the competing HER.
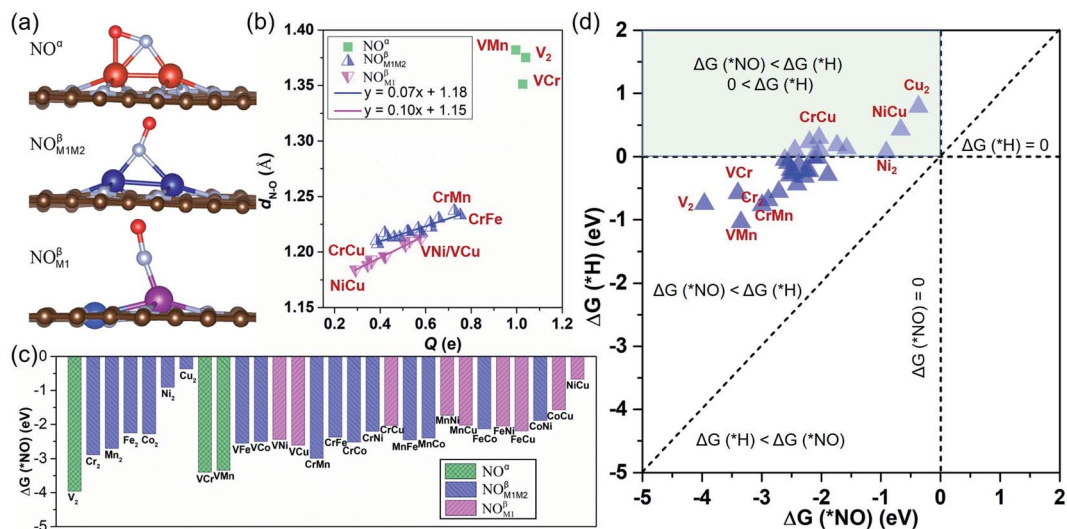
Fig. 2 (a) Side views of the three most stable adsorption configurations of NO over M1M2@NG DACs. (b) The relationship between the charge transfer (Q, e) and the N−O bond length (d_{N-O} (*NO), Å) of the most favorable *NO configurations on each M1M2@NG. Here, the positive values of Q indicate electron transfer from the catalyst to the adsorbed NO. (c) The free energy change (ΔG (*NO), eV) of the most stable *NO configuration over various DACs. (d) The ΔG for the *NO and *H over various DACs.

We then investigated the catalytic performances of the NORR over all DACs as most catalysts have a chemical adsorption ability for NO molecules. However, it's complex, cumbersome and resource-consuming work to consider all the reaction steps of the NORR for the 28 DACs that meet the first two rules (catalyst's stability and NO adsorption), which usually also occurred for other catalyst screening.[5,34,43] Thus, a one time and labor saving, and convenient method is an urgent need, which is significant for screening outstanding electrocatalysts for the NORR or multifunctional electrocatalysts for the NO$_x$RR.

From here obtained *NO configurations and previous studies,[19,57,61,62] we summarized the detailed reaction pathways for the NORR towards NH$_3$, as shown in Fig. 3. Given that the NO molecule contains N and O atoms, the proton–electron pairs can attack the N atom and also the O atom to produce NH$_3$ and H$_2$O, respectively. The sequential order of two product formation strongly depends on the NO adsorption configuration. Based on *NO with an end-on configuration, the reaction can follow O/N-distal and -alternating mechanisms to firstly form the product H$_2$O. Correspondingly, the NO reduction follows O/N-consecutive and -enzymatic mechanisms to firstly form either H$_2$O or NH$_3$. In particular, under the side-on *NO induced N-consecutive mechanism, protonation can lead to progressive hydrogenation of N atoms until NH$_3$ is preferentially formed with O atoms left over active sites. Moreover, the different reaction mechanisms can convert or hybridize with each other. We can find that no matter what mechanism the reaction follows, the first hydrogenation step is the *NOH/*HNO formation from *NO and the last hydrogenation step is the *NH$_3$ or H$_2$O formation, indicating that the NORR includes both the NRR and ORR features.

According to the results from calculating the entire reaction steps in recent studies about the NORR[19,61,62] and the similarity to the NRR,[32,63] the PDS for the NORR towards NH$_3$ may be the

stabilization of *NOH/*HNO species from NO adsorption (*NO → *NOH/*HNO), or destabilization of *NH$_2$ or *OH species to form the products (*NH$_2$ → *NH$_3$, or *OH → * + H$_2$O). Thus, the third screening criterion (Fig. 1b) for NORR activity consists of "two steps of key hydrogenation process", i.e., (1) *NO → *NOH/*HNO as the first procedure to select the catalyst candidates that meet the free energy threshold requirements (smaller than G_T of 0.40 eV) and (2) *NH$_2$ → *NH$_3$ or *OH → * + H$_2$O as the final procedure to confirm the NORR electrocatalyst with high activity. It is worth emphasizing that this reaction process always involves *NH$_3$ and H$_2$O formation, whether in the middle or at the last step. We thus simplified the final screening procedure for NORR activity to a combination of *NH$_2$ → *NH$_3$ and *OH → * + H$_2$O.

From the calculated free energy change as depicted in Fig. 4a, we can find that the first hydrogenation step (*NO → *NOH/*HNO) requires ΔG smaller than G_T (0.40 eV) over eight DACs (V$_2$, Cr$_2$, Cu$_2$, VCr, VMn, VFe, VCu, and CrMn), which are mostly V and Cr-based DACs (except for Cu$_2$). Among these DACs, the chemical adsorption of *NO upon hydrogenation forms stable intermediate *HNO or *NOH species with side-on configurations, except for VCu with an end-on configuration (Fig. S3†). The strong stabilization of *HNO or *NOH (only one for *NOH over VCr DAC) is responsible for the high activity for the *NO hydrogenation process. Here most of the DACs with small ΔG give rise to the more favorable *HNO than *NOH, different from that over transition-metal borides with more favorable *NOH.[61] Moreover, among these results, the N–O bond in *NO can break spontaneously by hydrogenation under ambient conditions, causing the smallest ΔG of the first hydrogenation step over V$_2$ (−2.03 eV) and VCr (−1.68 eV) DACs.

Through the first round of preliminary screening for NORR activity, we thus calculated the free energy change of *NH$_2$ → *NH$_3$ and *OH → * + H$_2$O over the above eight DAC candidates

9710 | J. Mater. Chem. A, 2022, 10, 9707–9716

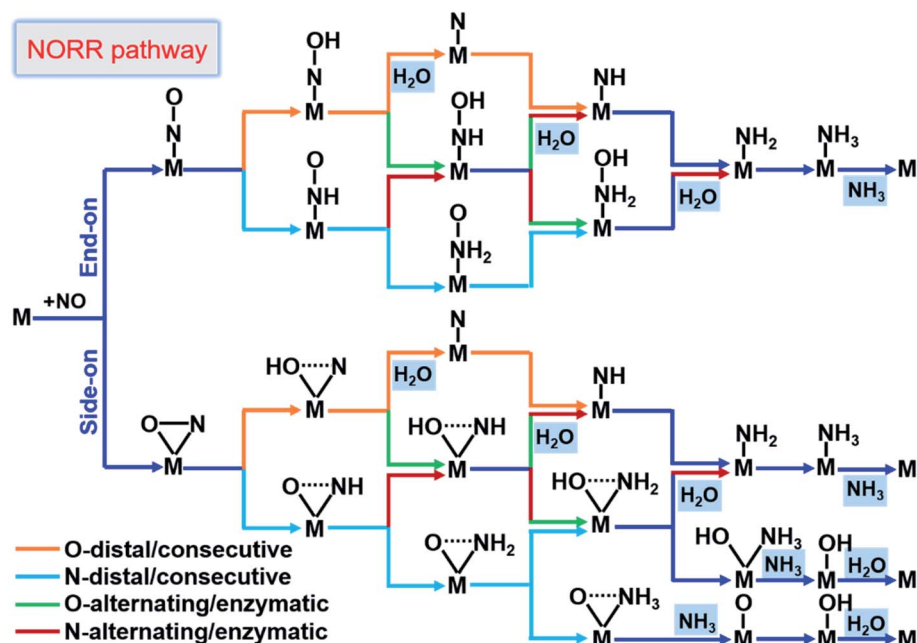This journal is © The Royal Society of Chemistry 2022

Fig. 3 Schematic depiction of the various pathways for the NORR towards NH_3. The dotted lines in the adsorbates indicate that bonds may be broken.

(Fig. 4b). It was found that only the Cu_2 DAC meets the screening metric of ΔG smaller than 0.4 eV, indicating that the Cu_2 DAC may show the greatest electroactivity for the NORR towards NH_3. The other seven DACs have a larger ΔG of H_2O formation (1.90 eV for V_2, 1.42 eV for Cr_2, 1.56 eV for VCr, 1.71 eV for VMn, 0.89 eV for VFe, 1.38 eV for VCu, and 1.10 eV for VMn), which is greater than that for $*NH_3$ formation and leads to the poisoning of active sites of DACs by $*OH$ species. A similar poisoning phenomenon also occurs for CO_2 reduction within low limiting potential for the Pd-based catalyst.[64]

A promising NORR electrocatalyst also requires good NH_3 selectivity, which suggests that it should have the ability to suppress the competing reaction to form the by-product. For example, at high potential, the NORR will lead to by-product (N_2O or N_2) formation on some metal surfaces.[14] For this reaction to occur, N–N coupling in the formation of N_2O_2 is required from two NO co-adsorbed on one active site. In consequence, as the first step in initiating the whole competing reaction, the affinity to $*NO$ (towards NH_3) and $*N_2O_2$ (towards N_2O and N_2) on catalysts will give rise to their reduction selectivity
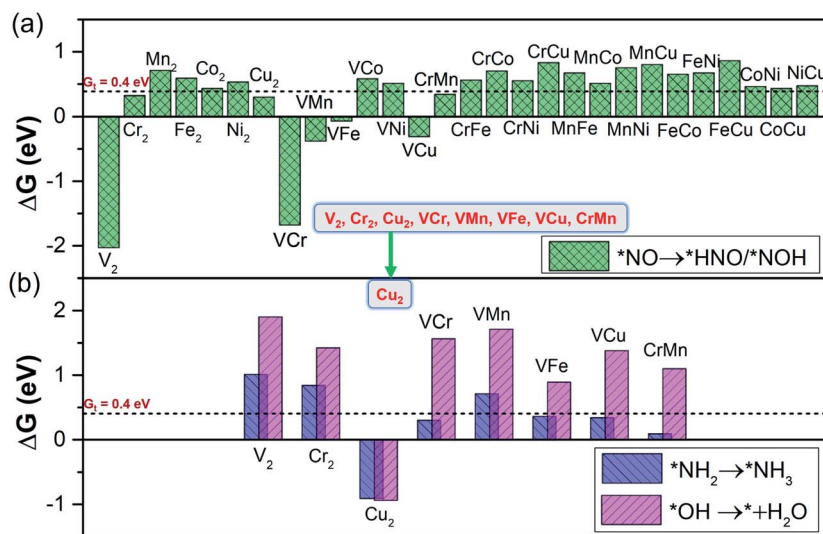

Fig. 4 The screening criterion of "two steps of key hydrogenation process" for NORR activity (step III in Fig. 1b), with the threshold value ($G_T =$ 0.40 eV). (a) The ΔG for stabilization of $*NOH/*HNO$ species ($*NO \rightarrow *NOH/*HNO$) over the 28 DACs. (b) The ΔG for destabilization of $*NH_2$ and $*OH$ species ($*NH_2 \rightarrow *NH_3$ and $*OH \rightarrow * + H_2O$) over the 28 DACs.

performance. We then compared their free energy changes for adsorption over the Cu_2 DAC, i.e., ΔG (*N_2O_2) vs. ΔG (*2NO). It was found that the *N_2O_2 formation from the NO dimer by N–N bond coupling (Fig. S4†) is unfavorable due to its less negative ΔG (−0.42 eV) than that for two separated *NO (−0.74 eV). This indicates that the two *NO prefer to separately adsorb on different active sites rather than on one site, which can suppress N_2O and N_2 formation.

To elucidate the results and verify our screening rule for NORR activity, we obtained the free energy diagrams of the most relevant pathway (the other pathways are also considered) for the NORR under zero and applied potential over Cu_2, VCr, VMn, VFe, VCu, and CrMn DACs, all of which have ΔG values smaller than 0.4 eV from *NH_2 to *NH_3. We can see that, over the Cu_2 DAC, the protonation of *H_2NO can firstly follow the N-consecutive mechanism to form *H_2NOH (Fig. 5a) and then transforms into an O-enzymatic mechanism to form the first product H_2O. Interestingly, *H_2NO species can also continuously follow the N-consecutive mechanism to form *ONH_3 that binds on the Cu site by an O–Cu bond, which firstly forms the product NH_3 and leaves the *O on the active site (Fig. 5b). The left *O over the Cu_2 DAC can be easily removed with small ΔG under ambient conditions via the protonation process: *O → *OH → * + H_2O. However, for VCr, VMn, VFe, VCu, and CrMn DACs, the high ΔG values (>0.8 eV) of *OH → * + H_2O induce the poisoning of active sites, despite the low ΔG values for the hydrogenation step of *NO, and *NH_2, and the other steps (Fig. S5†). These results well reveal that our screening criterion is effective and straightforward for NORR activity towards NH_3 and the Cu_2 DAC possesses the highest electrocatalytic activity with the lowest ΔG of 0.30 eV for the PDS (U_L = −0.30 V).

To gain insight into the high electrocatalytic activity of the Cu_2 DAC for the NORR, we revealed the intrinsic nature of the descriptor based on the d-orbital features of metal DACs, which may play an important role in the chemical and electrocatalytic activity. Based on the charge analysis of the scaling relationship with adsorption properties and free energy changes (for the details and results, see Note S4 with Fig. S14 in the ESI†) from 28 M1M2@NG DAC systems, here we found that the points for Cu-based DACs with more d electrons are concentrated in the region of higher electrocatalytic activity, though those for V and Cr-based DACs with fewer d electrons are relatively scattered in the region of lower electrocatalytic activity (Fig. 5c). This suggests that Cu-based DACs have more d electrons and thus higher electrocatalytic activity while V and Cr-based DACs with fewer d electrons induce their higher chemical activity (lower electrocatalytic activity), as observed elsewhere.[5,33] Thus, within reasonable limits, the $N_{d\text{-orbital}}$ can be a simple and approximate descriptor to evaluate the electrocatalytic activity of current DAC systems for the NORR, the determination of which does not need DFT calculations.

The classical Sabatier principle in catalysis determines that the adsorption energy of the reactants should be moderate. We also analyzed the appropriate affinity between *NO and the Cu_2 DAC using the charge density difference (CDD) and partial density of states (PDOS), as shown in Fig. 5d. The adsorption and activation of NO over metal catalysts depend on the

"acceptance–donation" mechanism,[20] which denotes that the metal–NO bond formation stems from the electron acceptance of empty metal-d orbitals from the NO-σ orbitals, and the elongation/activation of the N–O bond derives from the electron donation of metal-d orbitals to NO-π* orbitals. This "acceptance–donation" mechanism can be confirmed from the CDD of *NO over the Cu_2 DAC, where electron redistribution occurs upon NO adsorption with electron accumulation (purple region) and depletion (yellow region). Thus, the cooperation and reorganization of unoccupied and occupied d-orbitals of Cu-dimer activate the *NO. We can find the electronic state hybridization between Cu_2-d (purple) and NO-sp (blue) orbitals from the PDOS upon NO adsorption on the Cu_2 DAC. The d–π* orbital hybridization near the Fermi level indicates the activation of *NO, which induces low ΔG for the hydrogenation of *NO to from *HNO.

On the basis of pivotal NORR performance, it is necessary to explore multifunctional electrocatalysts that can also promote the electroreduction of NO_3^- and NO_2^- species to realize the NO_xRR towards NH_3 by protonation. To conduct the electrocatalytic NO_3RR and NO_2RR on catalysts, NO_3^- and NO_2^- species are expected to be adsorbed over the Cu_2 DAC, in view of the NO_3^- affinity of Cu surfaces.[65] We found that the Cu_2 DAC possesses moderate affinity for NO_3^- and NO_2^- species (Fig. 6a), which stems from the electron donation of the Cu_2 DAC to adsorbates with 0.78 and 0.66 electrons, respectively. Through free energy correction for the most stable *NO_3 and *NO_2 over the Cu_2 DAC, we obtained the ΔG (*NO_3) and ΔG (*NO_2) as −0.73 and −0.90 eV, smaller than that for *H (0.79 eV). From the CDD results, it was found that π* antibonding orbitals of NO_3^- and NO_2^- species accept electrons from the Cu_2 DAC, yielding the elongation of the N–O bond and activation of NO_3^- and NO_2^- species. Therefore, *NO_3 is promoted to accept the hydrogenation of O atoms to in turn generate *NO_2 and *NO. And *NO_2 is by means of two steps of hydrogenation to generate the *NO, then following by NORR to form the final product NH_3. The corresponding ΔG_{max} (U_L) for the NO_3RR to NH_3 (Fig. 6b) and the NO_2RR to NH_3 (Fig. 6c) is 0.36 (−0.36) and 0.32 eV (−0.32 V), comparable with 0.30 eV (−0.30 V) of the NORR to NH_3, revealing high NO_xRR activity with multifunctional electrocatalytic ability of the Cu_2 DAC.

We also performed the screening strategy on 4d (Rh, Pd, and Ag) and 5d (Ir, Pt and Au) late transition-metal based homonuclear DACs to search for suitable electrocatalysts for the NO_xRR, because these metal atoms have more d-orbital electrons with potentially high electrocatalytic activity. Through firstly the screening processes for NORR electrocatalysts, the DAC of Ag_2@NG was identified as the best one due to its small ΔG of the potential-determining step (0.14 eV) and high NH_3 selectivity (Table S1†). The free energy diagrams for the NORR towards NH_3 over the Ag_2 DAC via the most relevant mechanism are calculated (Fig. S6a†) and the corresponding structures of key steps along the reaction pathways are presented in Fig. S7.† Next, we obtained ΔG (*NO_3) and ΔG (*NO_2) as −0.73 and −0.74 eV, also smaller than that for *H (0.86 eV). The protonation of NO_3^- and NO_2^- species to NH_3 was studied (Fig. S6b and c†) and the corresponding ΔG_{max} (U_L) for the NO_2RR and

9712 | J. Mater. Chem. A, 2022, **10**, 9707–9716

This journal is © The Royal Society of Chemistry 2022

NO$_3$RR to NH$_3$ is 0.14 (-0.14) and 0.23 eV (-0.23 V), comparable with its electrocatalytic activity for the NORR to NH$_3$. Moreover, the result of deduced Ag$_2$@NG is added in Fig. 5c, and is located near the region of high electrocatalytic activity. This confirms that the Ag$_2$ DAC (Ag and Cu metal elements belong to the same group with more d-orbital electrons) also possesses high NO$_x$RR
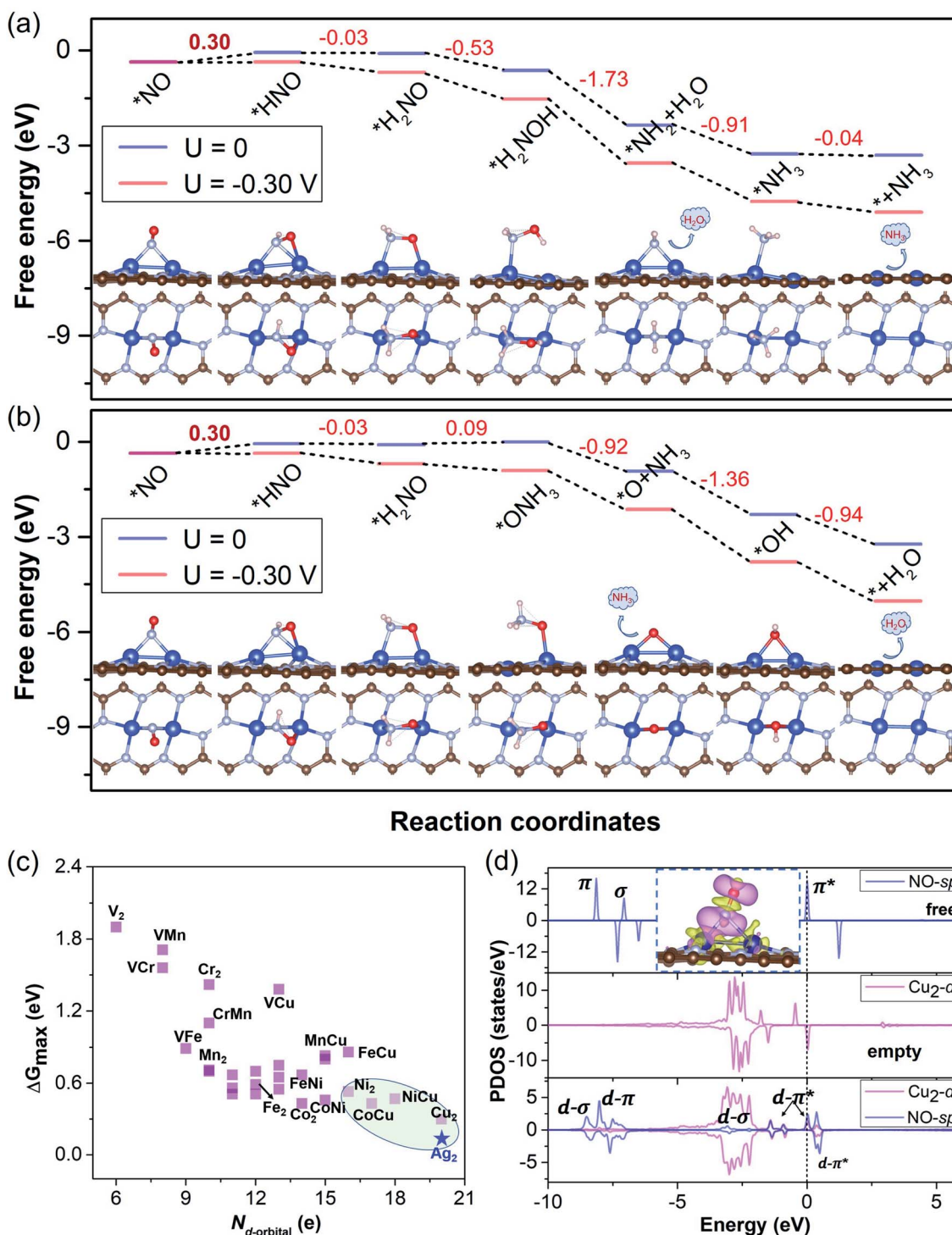

Fig. 5 (a and b) The free energy diagrams for the NORR towards NH$_3$ over the Cu$_2$ DAC *via* the two most relevant mechanisms. The corresponding free energy changes and structures of the key steps along the reaction pathways are presented and the ΔG_{max} values of the PDS are in bold. (c) The ΔG_{max} of the NORR *versus* the total number of d-orbital valence electrons ($N_{d\text{-orbital}}$) of free metal-dimer atoms (data from 28 M1M2@NG DAC candidates (M1/M2 = V, Cr, Mn, Fe, Co, Ni, and Cu)). (d) The PDOS with orbital interaction for the Cu$_2$ DAC, including the NO-sp orbitals for free NO molecules (blue), metal-d orbitals for Cu$_2$@NG without NO adsorption (purple), and metal-d orbitals and NO-sp orbitals for Cu$_2$@NG with NO adsorption, respectively. The Fermi level was set to 0. The inset shows the CDD (0.002 e Å^{-3}) for *NO over the Cu$_2$ DAC. The purple and yellow maps in the CDD denote electron accumulation and depletion, respectively.

This journal is © The Royal Society of Chemistry 2022

J. Mater. Chem. A, 2022, **10**, 9707–9716 | **9713**

Fig. 6 (a) The most stable configurations with the CDD (0.002 e Å^{-3}) for *NO$_3$ and *NO$_2$ over the Cu$_2$ DAC. The purple and yellow maps in the CDD denote electron accumulation and depletion, respectively. (b) The free energy diagrams for the NO$_3$RR towards NH$_3$ over the Cu$_2$ DAC. (c) The free energy diagrams for the NO$_2$RR towards NH$_3$ over the Cu$_2$ DAC. In (b) and (c), the corresponding free energy changes of the key steps along the reaction pathway are presented and the ΔG_{max} values of PDS are in bold.

activity with multifunctional electrocatalytic ability and again shows that our proposed screening strategy is feasible and efficient.

4. Conclusions

In summary, to investigate the multifunctional electrocatalytic ability of DACs for the NO$_x$RR towards NH$_3$, we firstly investigated the electrocatalytic activity of 28 DACs for the NORR by using the proposed strategy based on a first-principles screening method, which consists of the steps of "stability of catalyst", "NO adsorption", "NORR activity", and "NH$_3$ selectivity". Specifically, the "NORR activity" criterion includes two steps of key hydrogenation processes, *i.e.*, (1) *NO → *NOH/ *HNO and (2) *NH$_2$ → *NH$_3$ and *OH → * + H$_2$O, instead of considering the free energy changes for entire reaction steps. Through screening, our results reveal that the Cu$_2$@NG DAC is an excellent NORR electrocatalyst towards NH$_3$ with a rather low limiting potential of −0.30 V and great NH$_3$ selectivity, while its high electrocatalytic activity is also reflected in the NO$_2$RR (−0.32 V) and NO$_3$RR (−0.36 V) to identify the multifunctional electrocatalytic ability of Cu$_2$@NG. We also find a simple

descriptor of the total number of metal-dimer d-orbital valence electrons for electrocatalytic activity. The binding affinity of NO is deeply explained by the physical mechanism including the "acceptance–donation" mechanism and orbital interaction between the active metal of the catalyst and NO. The proposed strategy helps us to find another NO$_x$RR multifunctional electrocatalyst from 4d and 5d late transition-metal based DACs (Ag$_2$@NG). Our work effectively optimizes the screening strategy for the exploring of NO$_x$RR multifunctional electrocatalysts and gives an in-depth insight into the atomic mechanisms of NO$_x$ electroreduction.

Conflicts of interest

The authors declare no competing financial interest.

Acknowledgements

References

1 C. Ling, X. Niu, Q. Li, A. Du and J. Wang, *J. Am. Chem. Soc.*, 2018, **140**, 14161–14168.

2 X.-F. Li, Q.-K. Li, J. Cheng, L. Liu, Q. Yan, Y. Wu, X.-H. Zhang, Z.-Y. Wang, Q. Qiu and Y. Luo, *J. Am. Chem. Soc.*, 2016, **138**, 8706–8709.

3 T. Wang, Q. Liu, T. Li, S. Lu, G. Chen, X. Shi, A. M. Asiri, Y. Luo, D. Ma and X. Sun, *J. Mater. Chem. A*, 2021, **9**, 884–888.

4 C. Choi, S. Back, N.-Y. Kim, J. Lim, Y.-H. Kim and Y. Jung, *ACS Catal.*, 2018, **8**, 7517–7525.

5 D. Ma, Y. Wang, L. Liu and Y. Jia, *Phys. Chem. Chem. Phys.*, 2021, **23**, 4018–4029.

6 C. Liu, Q. Li, C. Wu, J. Zhang, Y. Jin, D. R. MacFarlane and C. Sun, *J. Am. Chem. Soc.*, 2019, **141**, 2884–2888.

7 J. Long, S. Chen, Y. Zhang, C. Guo, X. Fu, D. Deng and J. Xiao, *Angew. Chem.*, 2020, **132**, 9798–9805.

8 Y. Li, S. Xiao, X. Li, C. Chang, M. Xie, J. Xu and Z. Yang, *Mater. Today Phys.*, 2021, **19**, 100431.

9 Y. Zeng, C. Priest, G. Wang and G. Wu, *Small Methods*, 2020, **4**, 2000672.

10 J. Sun, D. Alam, R. Daiyan, H. Masood, T. Zhang, R. Zhou, P. J. Cullen, E. C. Lovell, A. Jalili and R. Amal, *Energy Environ. Sci.*, 2021, **14**, 865–872.

11 L. Li, C. Tang, X. Cui, Y. Zheng, X. Wang, H. Xu, S. Zhang, T. Shao, K. Davey and S. Qiao, *Angew. Chem.*, 2021, **133**, 2–9.

12 P. Gao, Z. Xue, S. Zhang, D. Xu, G. Zhai, Q. Li, J. Chen and X. Li, *Angew. Chem.*, 2021, **133**, 20879–20884.

13 R. Daiyan, T. Tran-Phu, P. Kumar, K. Iputera, Z. Tong, J. Leverett, M. H. A. Khan, A. Asghar Esmailpour, A. Jalili, M. Lim, A. Tricoli, R.-S. Liu, X. Lu, E. Lovell and R. Amal, *Energy Environ. Sci.*, 2021, **14**, 3588–3598.

14 H. Wan, A. Bagger and J. Rossmeisl, *Angew. Chem., Int. Ed.*, 2021, **60**, 21966–21972.

15 M. Duca and M. T. M. Koper, *Energy Environ. Sci.*, 2012, **5**, 9726–9742.

16 B. Qiao, A. Wang, X. Yang, L. F. Allard, Z. Jiang, Y. Cui, J. Liu, J. Li and T. Zhang, *Nat. Chem.*, 2011, **3**, 634–641.

17 Z. Wang, J. Zhao, J. Wang, C. R. Cabrera and Z. Chen, *J. Mater. Chem. A*, 2018, **6**, 7547–7556.

18 A. Wu, J. Yang, B. Xu, X.-Y. Wu, Y. Wang, X. Lv, Y. Ma, A. Xu, J. Zheng, Q. Tan, Y. Peng, Z. Qi, H. Qi, J. Li, Y. Wang, J. Harding, X. Tu, A. Wang, J. Yan and X. Li, *Appl. Catal., B*, 2021, **299**, 120667.

19 Q. Wu, B. Huang, Y. Dai, Y. Ma and T. Heine, ArXiv Prepr. arXiv211001947, 2021.

20 H. Niu, Z. Zhang, X. Wang, X. Wan, C. Kuai and Y. Guo, *Small*, 2021, **17**, 2102396.

21 L. Lv, Y. Shen, J. Liu, X. Meng, X. Gao, M. Zhou, Y. Zhang, D. Gong, Y. Zheng and Z. Zhou, *J. Phys. Chem. Lett.*, 2021, **12**, 11143–11150.

22 H. Niu, Z. Zhang, X. Wang, X. Wan, C. Shao and Y. Guo, *Adv. Funct. Mater.*, 2021, **31**, 2008533.

23 Y. Li, Q. Zhang, C. Li, H.-N. Fan, W.-B. Luo, H.-K. Liu and S.-X. Dou, *J. Mater. Chem. A*, 2019, **7**, 22242–22247.

24 W. Ren, X. Tan, W. Yang, C. Jia, S. Xu, K. Wang, S. C. Smith and C. Zhao, *Angew. Chem., Int. Ed.*, 2019, **58**, 6972–6976.

25 Y. Zhao, K. R. Yang, Z. Wang, X. Yan, S. Cao, Y. Ye, Q. Dong, X. Zhang, J. E. Thorne, L. Jin, K. L. Materna, A. Trimpalis, H. Bai, S. C. Fakra, X. Zhong, P. Wang, X. Pan, J. Guo, M. Flytzani-Stephanopoulos, G. W. Brudvig, V. S. Batista and D. Wang, *Proc. Natl. Acad. Sci. U. S. A.*, 2018, **115**, 2902.

26 Z. He, K. He, A. W. Robertson, A. I. Kirkland, D. Kim, J. Ihm, E. Yoon, G.-D. Lee and J. H. Warner, *Nano Lett.*, 2014, **14**, 3766–3772.

27 C. Wu, X. Zhang, Z. Xia, M. Shu, H. Li, X. Xu, R. Si, A. I. Rykov, J. Wang, S. Yu, S. Wang and G. Sun, *J. Mater. Chem. A*, 2019, **7**, 14001–14010.

28 T. He, A. R. P. Santiago, Y. Kong, M. A. Ahsan, R. Luque, A. Du and H. Pan, *Small*, 2021, 2106091.

29 Y. Cheng, S. He, J.-P. Veder, R. De Marco, S. Yang and S. Ping Jiang, *ChemElectroChem*, 2019, **6**, 3478–3487.

30 X. Lv, W. Wei, B. Huang, Y. Dai and T. Frauenheim, *Nano Lett.*, 2021, **21**, 1871–1878.

31 L. Zhang, G. Fan, W. Xu, M. Yu, L. Wang, Z. Yan and F. Cheng, *Chem. Commun.*, 2020, **56**, 11957–11960.

32 H. Li, Z. Zhao, Q. Cai, L. Yin and J. Zhao, *J. Mater. Chem. A*, 2020, **8**, 4533–4543.

33 X. Guo, J. Gu, S. Lin, S. Zhang, Z. Chen and S. Huang, *J. Am. Chem. Soc.*, 2020, **142**, 5709–5721.

34 D. Ma, Z. Zeng, L. Liu, X. Huang and Y. Jia, *J. Phys. Chem. C*, 2019, **123**, 19066–19076.

35 Z. W. Chen, J.-M. Yan and Q. Jiang, *Small Methods*, 2019, **3**, 1800291.

36 Z.-Y. Wu, M. Karamad, X. Yong, Q. Huang, D. A. Cullen, P. Zhu, C. Xia, Q. Xiao, M. Shakouri, F.-Y. Chen, J. Y. Kim, Y. Xia, K. Heck, Y. Hu, M. S. Wong, Q. Li, I. Gates, S. Siahrostami and H. Wang, *Nat. Commun.*, 2021, **12**, 2870.

37 G.-F. Chen, Y. Yuan, H. Jiang, S.-Y. Ren, L.-X. Ding, L. Ma, T. Wu, J. Lu and H. Wang, *Nat. Energy*, 2020, **5**, 605–613.

38 P. Li, Z. Jin, Z. Fang and G. Yu, *Energy Environ. Sci.*, 2021, **14**, 3522–3531.

39 W. Ye, S. Chen, Y. Lin, L. Yang, S. Chen, X. Zheng, Z. Qi, C. Wang, R. Long, M. Chen, J. Zhu, P. Gao, L. Song, J. Jiang and Y. Xiong, *Chem*, 2019, **5**, 2865–2878.

40 J. Wang, Z. Huang, W. Liu, C. Chang, H. Tang, Z. Li, W. Chen, C. Jia, T. Yao, S. Wei, Y. Wu and Y. Li, *J. Am. Chem. Soc.*, 2017, **139**, 17281–17284.

41 J. Wang, W. Liu, G. Luo, Z. Li, C. Zhao, H. Zhang, M. Zhu, Q. Xu, X. Wang, C. Zhao, Y. Qu, Z. Yang, T. Yao, Y. Li, Y. Lin, Y. Wu and Y. Li, *Energy Environ. Sci.*, 2018, **11**, 3375–3379.

42 X. Han, X. Ling, D. Yu, D. Xie, L. Li, S. Peng, C. Zhong, N. Zhao, Y. Deng and W. Hu, *Adv. Mater.*, 2019, **31**, 1905622.

43 T. Deng, C. Cen, H. Shen, S. Wang, J. Guo, S. Cai and M. Deng, *J. Phys. Chem. Lett.*, 2020, **11**, 6320–6329.

44 J. P. Perdew, K. Burke and M. Ernzerhof, *Phys. Rev. Lett.*, 1996, **77**, 3865.

45 G. Kresse and J. Furthmüller, *Phys. Rev. B: Condens. Matter Mater. Phys.*, 1996, **54**, 11169.

46 G. Kresse and J. Furthmüller, *Comput. Mater. Sci.*, 1996, **6**, 15–50.

This journal is © The Royal Society of Chemistry 2022

J. Mater. Chem. A, 2022, **10**, 9707–9716 | **9715**

47 S. Grimme, J. Antony, S. Ehrlich and H. Krieg, *J. Chem. Phys.*, 2010, **132**, 154104.

48 A. A. Peterson, F. Abild-Pedersen, F. Studt, J. Rossmeisl and J. K. Nørskov, *Energy Environ. Sci.*, 2010, **3**, 1311–1315.

49 J. K. Nørskov, J. Rossmeisl, A. Logadottir, L. Lindqvist, J. R. Kitchin, T. Bligaard and H. Jónsson, *J. Phys. Chem. B*, 2004, **108**, 17886–17892.

50 J. Rossmeisl, A. Logadottir and J. K. Nørskov, *Chem. Phys.*, 2005, **319**, 178–184.

51 http://webbook.nist.gov/chemistry/.

52 V. Wang, N. Xu, J.-C. Liu, G. Tang and W.-T. Geng, *Comput. Phys. Commun.*, 2021, **267**, 108033.

53 Y. Wang, X. Qin and M. Shao, *J. Catal.*, 2021, **400**, 62–70.

54 G. Brancato, N. Rega and V. Barone, *J. Chem. Phys.*, 2008, **128**, 144501.

55 K. Mathew, R. Sundararaman, K. Letchworth-Weaver, T. A. Arias and R. G. Hennig, *J. Chem. Phys.*, 2014, **140**, 084106.

56 G. J. Martyna, M. L. Klein and M. Tuckerman, *J. Chem. Phys.*, 1992, **97**, 2635–2643.

57 L. Zhang, J. Liang, Y. Wang, T. Mou, Y. Lin, L. Yue, T. Li, Q. Liu, Y. Luo, N. Li, B. Tang, Y. Liu, S. Gao, A. A. Alshehri, X. Guo, D. Ma and X. Sun, *Angew. Chem.*, 2021, **133**, 1–7.

58 X. Peng, Y. Mi, H. Bao, Y. Liu, D. Qi, Y. Qiu, L. Zhuo, S. Zhao, J. Sun, X. Tang, J. Luo and X. Liu, *Nano Energy*, 2020, **78**, 105321.

59 D. Kim, D. Shin, J. Heo, H. Lim, J.-A. Lim, H. M. Jeong, B.-S. Kim, I. Heo, I. Oh, B. Lee, M. Sharma, H. Lim, H. Kim and Y. Kwon, *ACS Energy Lett.*, 2020, **5**, 3647–3656.

60 S. L. Foster, S. I. P. Bakovic, R. D. Duda, S. Maheshwari, R. D. Milton, S. D. Minteer, M. J. Janik, J. N. Renner and L. F. Greenlee, *Nat. Catal.*, 2018, **1**, 490–500.

61 Y. Xiao and C. Shen, *Small*, 2021, 2100776.

62 Q. Wu, H. Wang, S. Shen, B. Huang, Y. Dai and Y. Ma, *J. Mater. Chem. A*, 2021, **9**, 5434–5441.

63 J. Zhao and Z. Chen, *J. Am. Chem. Soc.*, 2017, **139**, 12480–12487.

64 S. Chatterjee, C. Griego, J. L. Hart, Y. Li, M. L. Taheri, J. Keith and J. D. Snyder, *ACS Catal.*, 2019, **9**, 5290–5301.

65 T. Hu, C. Wang, M. Wang, C. M. Li and C. Guo, *ACS Catal.*, 2021, 14417–14427.

9716 | *J. Mater. Chem. A*, 2022, **10**, 9707–9716

This journal is © The Royal Society of Chemistry 2022